Human pose recovery using wireless inertial measurement units

2012 Physiol. Meas. 33 2099

(http://iopscience.iop.org/0967-3334/33/12/2099)

IOP PUBLISHING PHYSIOLOGICAL MEASUREMENT

Physiol. Meas. **33** (2012) 2099–2115 doi:10.1088/0967-3334/33/12/2099

Human pose recovery using wireless inertial measurement units

Jonathan F S Lin and Dana Kulić

Department of Electrical and Computer Engineering, University of Waterloo, Waterloo, ON, N2 L 3G1, Canada

E-mail: jf2lin@uwaterloo.ca and dkulic@ece.uwaterloo.ca

Received 20 July 2012, accepted for publication 5 November 2012
Published 23 November 2012
Online at stacks.iop.org/PM/33/2099

Abstract

Many applications in rehabilitation and sports training require the assessment of the patient's status based on observation of their movement. Small wireless sensors, such as accelerometers and gyroscopes, can be utilized to provide a quantitative measure of the human movement for assessment. In this paper, a kinematics-based approach is developed to estimate human leg posture and velocity from wearable sensors during the performance of typical physiotherapy and training exercises. The proposed approach uses an extended Kalman filter to estimate joint angles from accelerometer and gyroscopic data and is capable of recovering joint angles from arbitrary 3D motion. Additional joint limit constraints are implemented to reduce drift, and an automated approach is developed for estimating and adapting the process noise during online estimation. The approach is validated through a user study consisting of 20 subjects performing knee and hip rehabilitation exercises. When compared to motion capture, the approach achieves an average root-mean-square error of 4.27 cm for unconstrained motion, with an average joint error of 6.5°. The average root-mean-square error is 3.31 cm for sagittal planar motion, with an average joint error of 4.3°.

Keywords: human pose estimation, joint angle recovery, human motion analysis, rehabilitation, extended Kalman filter, forward kinematics

(Some figures may appear in colour only in the online journal)

1. Introduction

Human pose estimation is an important problem with many application areas, including human-computer interaction, rehabilitation and sports training. During the rehabilitation process, the therapist typically initiates each session by performing an assessment of the patient's current status, using visual observation of the patient's movement as well as questionnaires, e.g., the

Community Balance and Mobility Scale (Howe *et al* 2006). Following assessment, movement exercises are prescribed by a physiotherapist to help improve or recover muscle strength, endurance and range of motion. To ensure that such exercises are performed correctly and safely, the physiotherapist typically observes the patient while they perform the exercises. However, with the exception of goniometry, most of the exercise assessment tools available to the physiotherapist tend to be subjective in nature. Goniometry (Chao 1980, Jagodzinski *et al* 2000, Edwards *et al* 2004) is a human joint angle measurement technique that isolates a single body joint in order to assess a subject's range of motion (Norkin and White 2009). However, goniometrics cannot be employed accurately when the subject is moving, which reduces its usefulness during exercise or functional rehabilitation.

This research aims to develop an automated human motion measurement system capable of measuring arbitrary three dimensional motion, to enable applications such as automated patient assessment and monitoring during knee and hip rehabilitation. The proposed system uses lightweight inertial measurement unit (IMU) packages, which can be mounted non-invasively onto the patient via Velcro straps. The linear acceleration and angular velocity data generated by the sensors can be used to characterize the patient's movement during the performance of the rehabilitation exercises, and to provide feedback to the patient and therapist, even when the patient is moving. Source-less IMUs are favored over camera, acoustic or mechanical based motion detection due to size, cost and environment concerns (Zhou *et al* 2008). The use of ambulatory sensors also enables applications in outdoor settings for sports training. However, using IMUs to obtain an accurate estimate of the joint angles is a challenging problem.

Many of the existing works in the field utilize accelerometers as inclinometers to measure knee angles. Often, the operational space is simplified, and motions are only examined in a 2D sagittal plane. For slow motions, the acceleration contributed by the subject's motion is assumed to be negligible compared to gravity. Trigonometry is applied to the acceleration signal to obtain the incline of the accelerometer. Bergmann *et al* (2009) used accelerometers in this manner to obtain the incline of the knee and ankle. They showed that this algorithm produces comparable accuracy to joint angles determined by a motion capture system. However, when the motion is fast, it is difficult to determine which component of the acceleration is caused by motion, and which is caused by gravity. Dong *et al* (2007) proposed using two accelerometers per link segment and combined them into a virtual accelerometer at a common location in order to use the difference in the accelerometers' readings to mathematically remove the link velocity. This approach required two sensors per joint, making it cumbersome to use. In general, using accelerometers alone to estimate joint angles is a limited solution, since this approach can only determine the link incline for joints moving in a plane perpendicular to gravity.

Gyroscopes can be added to accelerometers to improve accuracy and handle fast and out-of-plane motions. However, gyroscopes can also introduce additional difficulties, particularly the gyroscopic drift[1]. Williamson and Andrews (2001) employed accelerometers during stationary or slow-moving situations to obtain the knee joint angle. When the variance of the accelerometers reached a certain threshold, the angle determination was calculated by the integration of the gyroscope instead. This allows the gyroscope to be employed in fast-moving situations, and also resets the drift error by switching to the accelerometer signal on a regular basis. This direct gyroscope integration is commonly known as *strapdown integration* (King 1998). Williamson's system was used to recover sagittal knee angle in a sit-to-stand task, and showed improvements over accelerometer-only setups. However, this approach would only

[1] Gyroscope calibration is often imperfect and a non-zero dc bias is introduced into the sensor reading, producing a non-zero angular velocity measurement when no motion is actually occurring. When integrated, the estimated position diverges.

work with rhythmic motions, where stops are frequent. For a long motion, the integrator would not have a chance to reset, increasing the impact of drift on the joint estimates.

Boonstra *et al* (2006) determined the incline of the thorax, the upper leg and the lower leg by taking the arctangent of the accelerometer, integrating the gyroscope data and combining the two results. The acceleration signal was low-pass filtered to reduce sensor noise, while the gyroscope signal was high-pass filtered to reduce the dc offset. This arrangement is also known as the *complementary filter* (Higgins 1975). Boonstra's implementation does not recover joint angles, but sagittal incline. Although the above approaches showed good accuracy in 2D motion analysis in the sagittal plane, it is not trivial to generalize these algorithms to handle 3D motion, as all of these algorithms rely on the assumption that the motion is constrained in the gravity-acting plane, so that the accelerometer can be used as an inclinometer.

Luinge and Veltink (2005) utilized strapdown integration in a Kalman filter framework. A set of IMUs were placed on the pelvis, trunk and forearm. Gyroscope data was used to generate the rotational matrices for the motions of each body segment, and allow the direction of gravity in the sensor frame to be identified. A gyroscope dc bias term was also included as a state in the Kalman filter, to control the gyroscopic drift. Although Luinge's implementation is capable of generating estimates of the full 3D rotation of each body segment with respect to the world frame, only the body segment incline and heading are evaluated in the paper. Luinge's algorithm treats each body segment as an independent rigid body, without considering any kinematic relationships or mobility constraints between body segments. This means that position and orientation estimates for adjacent body segments may drift and move with respect to each other in ways that are not physically realizable.

Zhou *et al* (2008) also utilized strapdown integration to obtain the joint rotation of each link. Unlike previous works, they subtracted out the gravity vector, as opposed to relying on it to obtain the link incline. They obtained joint end-effector location by double-integrating the gravity-subtracted acceleration signal to obtain position. To reduce the impact of integration drift on the end-effector calculation, Lagrangian optimization was applied with kinematic constraints. Although they had a mechanism for dealing with accelerometer integrational drift, they do not have an explicit method for handling gyroscopic integrational drift.

In addition to accelerometers and gyroscopes, magnetometers can also be used to provide orientation information (e.g. Zhu and Zhou 2004). One drawback of using magnetometers is that the magnetometer is sensitive to local fluctuations of the Earth's magnetic field that occur when ferromagnetic materials are nearby. A local magnetic field can be introduced (Roetenberg *et al* 2007) but requires additional equipment to be mounted on the patient, which is undesirable.

Commercial systems have also recently been introduced (Roetenberg *et al* (2009)'s Xsens MVN[2], Animazoo IGS series[3], or the Biosyn FAB[4]). However, these commercial solutions may not be well suited for physiotherapy applications. These solutions tend to be expensive, and require a long calibration routine, which may not be possible for patients who have difficulty moving. Suit size and fit is also a concern, especially as obesity is a risk factor for many musculoskeletal injuries. Furthermore, equipment cleaning is nontrivial, especially for the suit-based products.

In this paper, an algorithm to estimate arbitrary 3D human motion is proposed. Small and light-weight IMU sensor packages attached to the knee and ankle are used to wirelessly transmit the patient's acceleration and gyroscope profile during motion. Using a kinematic model, the sensor information is fused with an extended Kalman filter (EKF). Kinematic

[2] Xsens Technologies, www.xsens.com
[3] Animazoo Ltd., www.animazoo.com
[4] Biosyn Systems, www.biosynsystems.net

constraints and filter noise adaptation are employed to reconstruct the joint angles of the subject. The proposed system is capable of recovering the leg pose in terms of joint angles during arbitrary 3D motion. This is a significant improvement over existing works based on incline angles in the sagittal plane, which are incapable of providing 3D angle recovery.

Most of the existing works implement body segment orientation estimation without the use of kinematic constraints (e.g. Boonstra *et al* (2006), Luinge and Veltink (2005)). This allows these algorithms to be applied on any arbitrary object and determine its orientation with respect to the world frame. However, human kinematics constrains the possible movements that can be physically realized. These constraints should be considered to improve joint angle estimates, such as the knee joint's inability to perform abduction motion. By utilizing a kinematic model in our algorithm, we realistically constrain the space of possible motions, and provide a more accurate estimate of joint angles.

Without a kinematic model, these algorithms also cannot provide joint angle estimates. Instead, they provide orientation estimates relative to the world frame, such as incline angle from ground or heading angle from the vertical. To produce more clinically relevant information, the estimated orientations must be converted to joint angles by incorporating kinematic information in a post-processing step. By incorporating the kinematic information directly into the estimation process, our algorithm produces the joint angle data of interest directly and improves robustness against drift.

2. Proposed approach

In order to estimate the human pose during physiotherapy motions, IMU sensors are attached to the knee and ankle of the patient. The IMU data are combined to determine joint angles based on a kinematic model and an EKF.

2.1. Forward kinematics

To derive a kinematic model of the lower body, we model the human leg as an articulated chain of rigid bodies, where each rigid body corresponds to a leg limb. The rigid bodies (limbs) are connected through a set of joints (i.e. the hip, knee and ankle). To construct the kinematic model, a reference frame (denoted as the ith frame) is attached to each DoF (denoted as the $i-1$th joint) following the Denavit–Hartenberg (DH) convention (Uicker *et al* 1964). DH convention, a framework initially developed for robot manipulator analysis, is very useful as it provides a framework for modeling any articulated chain of rigid body links by modeling the system mobility as a series of single degrees of freedom (DoF) joints. The DH frame assignments for the model used in this paper are illustrated in figure 1, and are described as follows: frames 0, 1 and 2 correspond to the 3 DoFs at the hip, and are located at the hip origin, forming a 3 DoF spherical joint at the hip. Offset from the first three frames by the length of the upper leg, frames 3 and 4 form a 2 DoF revolute/rotational joint at the knee, allowing for knee flexion/extension, as well as internal/external rotation. Frame 5 is offset from frames 3 and 4 by the length of the lower leg, and is the last frame of this kinematic chain. Homogeneous transformations are utilized to rotate between the DH frames and the local sensor frames.

For simplicity, we assume frame 0 to be stationary, so for motions where the foot is not moving, such as sit-to-stand, the kinematic chain is reversed, such that the ankle is the 3 DoF joint, and the knee remains as the 2 DoF joint. Although the current formulation requires a stationary base frame, the proposed algorithm can be extended to motions that do not have a fixed base, by accounting for the base frame motion in the state vector. This is a common technique in the robotics field, and has been applied to the analysis of mobile manipulators. The

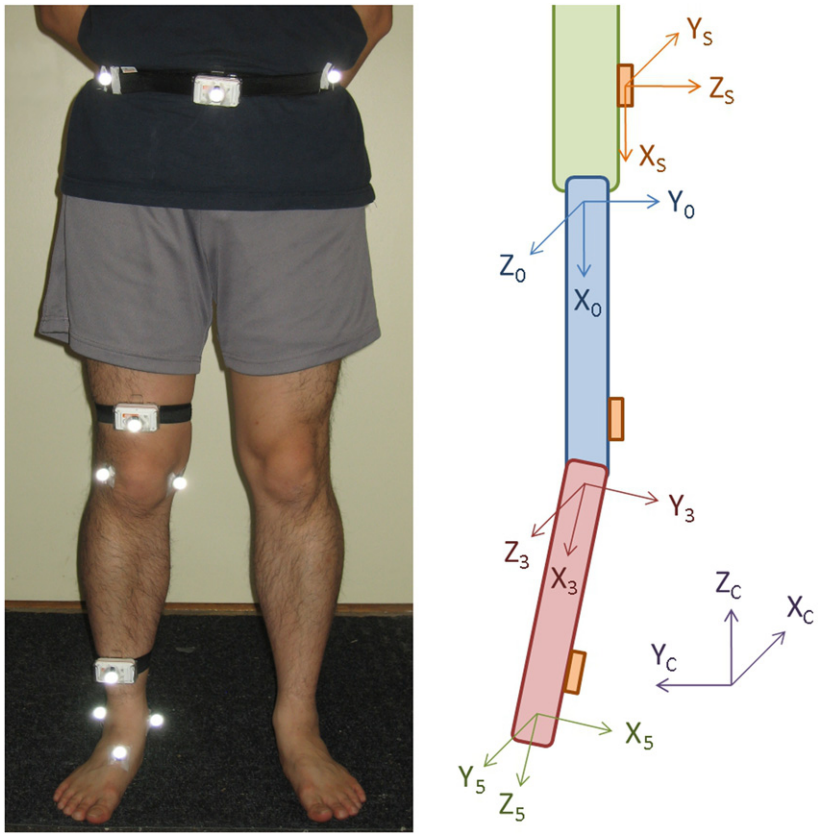

Figure 1. The hip is modeled as 3 rotational DoFs, and the knee and shin are modeled as 2 DoFs. Frames 0–5 are assigned by DH convention. SHIMMER sensors, containing the accelerometers and gyroscopes, were positioned on the hip, knee and ankle of the participant. (Left) An image of the sensors on a participant's hip, knee and ankle. Motion capture markers placements are also shown. (Right) A profile image of the torso, upper and lower leg, rotated 90° from the left image. Frame 0, 3 and 5 refers to the hip, knee and ankle starting frames, respectively. Frame 1, 2 and 4 correspond to intermediate hip and knee DoF frames, and are not shown for brevity. The boxes on the leg represents the sensor packages. Frame 0 is the reference frame where the errors are assessed. The S frame indicates the local frame of the sensor, and is identical for all sensors. The C frame represents the global frame of the motion capture system.

motion of the base can be estimated within the same Kalman filter framework by incorporating data from a sensor that experiences only the base frame movement, such as the sensor located at the waist. This approach would also allow both arm and foot motions to be modeled using the waist as the origin of the moving base frame, and using additional sensors located at the elbow and shoulder.

Given a DH frame assignment, the forward kinematics of any articulated chain can be computed by successively applying the frame transformations (Spong *et al* 2006). Given the angular velocity of the preceding frame, ω_{i-1}^{i-1}, and the joint velocity $\dot{q}_i$, generated by joint i, we can compute the resulting angular velocity ω_i^i of the next frame:

$$\omega_i^i = R_{i-1,i}^T \omega_{i-1}^{i-1} + R_{i-1,i}^T \dot{q}_i. \tag{1}$$

This formulation allows the angular velocity of each segment to be determined recursively, by looking only at the motion of the current link (the ith frame) and the link immediately previous to it (the $i-1$th frame). We include the angular velocity ω generated by joint $i-1$ (describing the velocity between frames $i-1$ and i), by rotating the angular velocity into the current frame with a rotation matrix $R_{i-1,i}$. $R_{i-1,i}$ can be derived from the DH frame definition.

The angular velocity is differentiated to obtain the angular acceleration α_i^i:

$$\alpha_i^i = R_{i-1,i}^T \alpha_{i-1}^{i-1} + R_{i-1,i}^T \ddot{q}_i + \omega_i \times \left(R_{i-1,i}^T \dot{q}_i\right). \tag{2}$$

The linear velocity of the current frame $\dot{x}_i$ is obtained by computing the cross-product of the angular velocity and displacement vector from the center of the current frame to the center of the previous frame, r_i:

$$\dot{x}_i = R_{i-1,i}^T \dot{x}_{i-1} + \omega_i^i \times r_i. \tag{3}$$

Differentiation is carried out again to obtain the linear acceleration, $\ddot{x}_i$:

$$\ddot{x}_{i,i} = R_{i-1,i}^T \ddot{x}_{e,i-1} + \alpha_i^i \times r_i + w_i^i \times (w_i^i \times r_i) \tag{4}$$

$$\ddot{x}_{e,i} = R_{i-1,i}^T \ddot{x}_{e,i-1} + \alpha_i^i \times r_i + w_i^i \times \left(w_i^i \times r_i\right) + R_{0,i} g. \tag{5}$$

In equation (4), the first term represents the acceleration transmitted from the previous frame, while that the second and third terms in the $\ddot{x}$ represent the tangential and radial acceleration, respectively. An extra term, $R_{0,i}g$ is added to equation (5) (describing the end effector acceleration) in order to model the gravity term g, and to rotate it into the local frame.

The position of each sensor can be obtained by rotating all the link lengths preceding the sensor into frame 0, and adding them:

$$x_{e,\text{upper}} = R_{0,3} r_{1S} \tag{6}$$

$$x_{e,\text{lower}} = R_{0,3} r_{12} + R_{0,5} r_{2S} \tag{7}$$

where $x_{e,\text{upper}}$ and $x_{e,\text{lower}}$ are the Cartesian coordinates of the knee and ankle respectively. r_{1S} is the vector from the hip origin to the location of the sensor on the upper leg. r_{12} is the vector from the hip to the knee. r_{2S} is the vector from the knee to the sensor on the lower leg. The r link information can be obtained by surface anthropometric measurement of bony landmarks (Norkin and White 2009). This can be done with tape measure, or motion capture markers.

Using the DH convention shown in figure 1, frames 0, 1 and 2 are located at the hip, and describe the motions of the thigh. q_{1-3}, $\dot{q}_{1-3}$ and $\ddot{q}_{1-3}$ describe the joint angles, angular velocities and accelerations of the 3 DoFs in the hip joint. We assume that the base frame is stationary, $\ddot{x}_{e,0} = \alpha_0^0 = \omega_0^0 = 0$, and thus $\omega_1 = \dot{q}_1$ and $\alpha_1 = \ddot{q}_1$. $\ddot{x}_{e,3}$ describes the linear acceleration of the knee, and is measured by the knee accelerometer. ω_3 is measured by the knee gyroscope. Since frames 0 and 1 share the same origin, and thus have no link offset, $\ddot{x}_{1-2} = 0$.

Frames 3 and 4 are located at the knee, and describe the motion of the lower leg. q_{4-5}, $\dot{q}_{4-5}$ and $\ddot{q}_{4-5}$ describe the joint angles, angular velocities and accelerations of the 2 DoFs in the knee joint. Unlike the upper leg, the lower leg has the upper leg as a previous frame, thus ω_5 and α_5 describe the angular velocities/accelerations of both the lower leg itself, as well as the angular velocities/accelerations transmitted from the upper leg. Similar to the previous segment, $\ddot{x}_{e,5}$ describes the linear acceleration of the ankle, measured by the ankle accelerometer, whereas ω_5 is measured by ankle gyroscope.

2.2. Extended Kalman filter

The Kalman filter (Welch and Bishop 2006) is a sensor fusion technique that estimates system state from noisy observations, assuming that a linear state and observation model are known, and that both process and measurement noise are zero mean Gaussian functions. For the standard Kalman filter, the state estimate s_t and observation update z_t are defined as:

$$s_t = As_{t-1} + w_{t-1} \tag{8}$$

$$z_t = Cs_t + v_t. \tag{9}$$

The matrix A in equation (8) is the process update equation that relates the previous state of the system s_{t-1} to the current state s_t. The process noise w is assumed to be zero-mean and Gaussian, with a covariance Q. The matrix C in equation (9) is the measurement update equation, relating the current state s_t to the measurement vector z_t. v is the measurement noise, and is also assumed to be zero-mean and white, with a covariance of R.

The Kalman filter assumes linear process and measurement equations, however the forward kinematic equations derived in equation (1) and (4) from section 2.1 do not satisfy this assumption. For non-linear systems, the EKF (Welch and Bishop 2006) can be utilized. The EKF linearizes the nonlinear equations via first-order Taylor expansion, and utilizes the linearized function in the Kalman filter.

The goal of the proposed approach is to estimate the joint angles q_i based on the measurements obtained from the accelerometers and gyroscopes, $\ddot{x}_{e,3}$, ω_3, $\ddot{x}_{e,5}$, ω_5. The system state therefore consists of the joint angles, velocities and accelerations, q_i, $\dot{q}_i$ and $\ddot{q}_i$. The following kinematic motion equations are used as the process (state) model:

$$q_t = q_{t-1} + \dot{q}t + \ddot{q}t^{2/2} \tag{10}$$

$$\dot{q}_t = \dot{q}_{t-1} + \ddot{q}t \tag{11}$$

$$\ddot{q}_t = \ddot{q}_{t-1}. \tag{12}$$

This system model includes the evolution of position and velocity, while acceleration is modeled to remain constant. The unmodeled higher order terms (i.e. changes in acceleration) are accounted for through the inclusion of process noise. Note that this modeling approach requires that the process noise be modified depending on the motion speed, as the impact of the unmodeled higher values would become more significant at higher speeds, and thus Q would need to be increased accordingly. This issue is handled through the automatic tuning of the process noise parameters, as described in section 2.3.

Since all the equations are already linear, the A matrix is straightforward to formulate:

$$A = \begin{bmatrix} 1 & t & t^2/2 \\ 0 & 1 & t \\ 0 & 0 & 1 \end{bmatrix}. \tag{13}$$

Equations (1) and (4) are used as the measurement equations, which are nonlinear. They can be written in a general form: $z_t = h(s_t, v_t)$, where h is the nonlinear function to produce z_t. The measurement equation is linearized as follows:

$$z_t \approx \tilde{z}_t + C(s_t - \tilde{s}_t) + Vv_t \tag{14}$$

where C is the Jacobian matrix of the partial derivatives of the measurement equations h with respect to the state s, $\tilde{s}$ is the noise-less state estimate, and V is the Jacobian matrix of partial derivatives of h with respect to the measurement noise v. We assume Gaussian measurement noise, so that $V = I$, where I is the identity matrix. The formulation of the EKF is as follows (Welch and Bishop 2006):

$$\hat{s}_t^- = As_{t-1} \tag{15}$$

$$P_t^- = AP_{t-1}A^T + W_tQ_{t-1}W_t^T \tag{16}$$

$$P_y = C_tP_t^-C_t^T + V_tRV_t^T \tag{17}$$

$$K_t = P_t^-C^T(P_y)^{-1} \tag{18}$$

$$\hat{s}_t = \hat{s}_t^- + K_t\left(z_t - h\left(\hat{s}_t^-, 0\right)\right) \tag{19}$$

$$P_t = (I - K_tC_t)P_t^-. \tag{20}$$

These equations can be separated into *a priori* and *a posteriori* equations, indicating operations before and after the incorporation of the measurement update step. The *a priori* state $\hat{s}_t^-$ and error covariance P_t^- are estimated by equations (15) and (16) respectively, and are based on the state of the previous timestep, s_{t-1}^-. The current measurement, z_t, is incorporated into the Kalman gain calculation in equation (18), allowing for the calculation of the *a posteriori* state $\hat{s}_t$ and error covariance P_t in equations (19) and (20) (Welch and Bishop 2006). This approach automatically addresses the issue of gravity contamination. Gravity is modeled in the EKF measurement equation (5), and assuming that the state is properly recovered by the EKF, allowing for the correct set of rotational matrices to be constructed, the gravity contamination problem is effectively addressed, without imposing any constraints on the motion speed.

2.3. Adaptation of the noise parameters

As noted in section 2.2, the process noise w needs to increase and decrease based on the speed of motion, in order to account for unmodeled higher order terms in the process equations. Also, if the measurement noise v is improperly modeled, equation (14) is not able to properly account for the sensor noise, and integrational drift will occur. This paper proposes an automated approach for process noise tuning to address these issues.

Poor selection of the process noise w can significantly impact the performance of the filter. If it is too small, the higher order terms that are not modeled in the A matrix cause improper state estimation. If it is too high, too much noise is injected into the state estimate. Both of these situations could affect the state and state variance estimates, causing the EKF intermediate matrices to become poorly conditioned. In particular, the calculation of the Kalman gain in equation (18) requires the matrix inversion of the P_y term. The measurement equation C is a function of the state. Thus, if a poor w selection leads to poor state recovery, P_y can become poorly conditioned. The matrix inversion of a poorly conditioned matrix causes numerical errors, and can cause the EKF algorithm to diverge.

Since the goal is to develop an online estimation algorithm, an approach to automatically detect poor conditioning in the covariance matrix and prevent EKF divergence is needed. When P_y is approaching a singularity, the filter state is reset to the initial values, since a near-singular P_y matrix can introduce erroneous results into the states. After the filter has been reset, the process covariance is increased to reduce the chances of future singularities. The initial process noise parameters can be selected to be low, and be increased gradually by this tuning process until the proper process noise is found.

It is, however, difficult to set a threshold $\epsilon_{\text{divThres}}$ for the poorly conditioned matrix. The condition number of the P_y matrix fluctuates based on the state estimates, and can naturally become high and low. Since it is undesirable to accidentally reset the filter or change the noise profile while the filter is working as expected, a high value for $\epsilon_{\text{divThres}}$ was set, so that the auto-tuning code would only be triggered right before P_y becomes singular. As a result, by the time the condition number of P_y exceeds the threshold, the recovered angles are likely to have been inaccurately estimated for several timesteps. A timestep rewind is applied so that

the updated filter will overwrite these poorly estimated states. It may also be possible that the joint angles become exceedingly large before the condition numbers are overtly impacted. Therefore, if a given joint exceeds its corresponding joint limit, q_c, by a factor, the filter is also reset. This process is summarized in algorithm 1.

Algorithm 1 Process noise auto-tune algorithm.

if $\text{cond}(P_y) \geqslant \epsilon_{\text{divThres}} \parallel q \gg 3q_c$ **then**
  Rewind timesteps
  Reset filter state
  Increase process noise w
end if

2.4. Kinematic constraints

Poor selection of measurement noise v can also impact filter performance. If v is too small, the measurement equations cannot adequately account for the amount of noise that is in the sensor data, causing integrational drift. If v is too high, motion data may be lost as it is being discarded by the EKF as noise. However, unlike the process noise, where poor selection could cause singularities, it is difficult to determine if the signal is drifting or if the movement is natural. However, natural motion is constrained by the human joint angle ranges, and cannot exceed them, whereas a drifting signal would grow without bound.

To incorporate knowledge of the range of motion constraints to reduce drift, the estimated state angles are checked at each timestep to ensure that they are within realistic bounds. A potential field (Khatib 1985) is applied to push q away from joint bounds. The potential field generates a virtual acceleration pushing the joint away from the joint boundary whenever the joint is close to the joint limit. Given

$$\underline{\rho}_i = q_i - \underline{q}_{c,i} \tag{21}$$

$$\overline{\rho}_i = \overline{q}_{c,i} - q_i \tag{22}$$

the potential field acceleration γ_i is calculated by

$$\gamma_i = \begin{cases} \eta \left(\dfrac{1}{\underline{\rho}_i} - \dfrac{1}{\underline{\rho}_{0,i}} \right) \dfrac{1}{\underline{\rho}_i^2} & \text{if } \underline{\rho}_{\text{i}} \leqslant \underline{\rho}_{0,\text{i}} \\ -\eta \left(\dfrac{1}{\overline{\rho}_i} - \dfrac{1}{\overline{\rho}_{0,i}} \right) \dfrac{1}{\overline{\rho}^2} & \text{if } \overline{\rho}_{\text{i}} \leqslant \overline{\rho}_{0,\text{i}} \\ 0 & \text{otherwise} \end{cases} \tag{23}$$

where $\underline{q}_{c,i}$ and $\overline{q}_{c,i}$ are the lower and upper bound on the joint q, and $\underline{\rho}_{0,i}$ and $\overline{\rho}_{0,i}$ are the distance limits of the potential field influence. η is the potential field coefficient. As q_i approaches the joint constraint $q_{c,i}$, γ_i applies an increasingly large acceleration in the opposite direction to push the joint back within the acceptable range. The pseudocode for this process is described in algorithm 2.

Table 1. Participant anthropometric data. All lengths in (cm), all weights in (kg). l_u is the hip-to-knee length. l_{usl} is the length along the upper leg to the knee sensor. l_{usr} is the radius of the upper leg at the knee sensor. l_l is the knee-to-ankle length. l_{lsl} is the length along the lower leg to the ankle sensor. l_{lsr} is the radius of the lower leg at the ankle sensor.

	Height	Weight	Age	l_u	l_{usl}	l_{usr}	l_l	l_{lsl}	l_{lsr}
Mean	168.7	65.2	23.3	44.8	34.9	7.2	38.2	23.4	6.5
Std. Dev.	9.2	10.1	3.5	4.3	6.1	1.5	2.5	4.7	0.6
Max	183.0	90.0	31.0	57.3	47.0	12.0	43.4	32.1	8.2
Min	150.0	47.7	19.0	37.4	22.7	5.2	33.9	14.4	5.3

Algorithm 2 Kinematic constraining algorithm.

for $i = 1 \rightarrow 5$ **do**
  $\overline{\rho}_i \leftarrow \overline{q}_{c,i} - q_i$
  $\underline{\rho}_i \leftarrow q_i - \underline{q}_{c,i}$
  if $\overline{\rho}_i \leqslant \overline{\rho}_{0,i}$ **then**
    $\ddot{q}_{t,i} \leftarrow -\eta(1/\overline{\rho}_i - 1\overline{\rho}_{0,i})/\overline{\rho}_i^2$
  else if $\underline{\rho} \leqslant \underline{\rho}_0$ **then**
    $\ddot{q}_{t,i} \leftarrow -\eta(1/\underline{\rho}_i - 1\underline{\rho}_{0,i})/\underline{\rho}_i^2$
  else
    $\ddot{q}_{t,i} \leftarrow A\ddot{q}_{t-1,i}$
  end if
end for

The proposed joint limit algorithm can be used to constrain the joint angle estimates to anthropometrically feasible values in the case of arbitrary 3D motion. If additional information is available about the motion to be performed, the joint limits can be modified to include this additional information. For example, for the case of motion in the sagittal plane only, joint angle limits for out of plane joints can be decreased to incorporate this additional information into the filter and further reduce drift error.

3. Experiments

The proposed algorithm was tested against motion capture data. All signal processing, algorithmic implementation and error calculations were programmed in MATLAB 7.12. The EKF functions were implemented with the ReBEL MATLAB Toolbox from Wan and Nelson (2001).

3.1. Data collection

The algorithm was tested on healthy subjects performing typical knee and hip rehabilitation movements. The movement data of 20 participants (12 M, 8 F) were collected, with the average participant being 23 years old. No participant had any lower back or leg injuries in the past six months. The experiment was approved by the University of Waterloo Research Ethics Board, and signed consent was obtained from all participants. Participant anthropometric data are summarized in table 1, and are derived from motion capture data.

Table 2. Exercise descriptions for rehabilitation exercises.

Name	Initial pose	Description
Knee flexion (KF)	Seated	Knee extension/flexion.
Sit to stand (SS)	Seated	Stand up from a seated posture.
Squats (SQ)	Standing	While keeping upper body upright, bend knees to lower torso vertical position.
Hip-knee flexion (HF)	Lying down	Starting with the leg straight, bend at the knee and hip to slide the heel toward the buttocks.
Straight leg raise (SL)	Lying down	Keeping the leg straight, bend at the hip and lift the entire leg up from the ground.

Table 3. Exercise descriptions for out-of-plane motions.

Name	Initial pose	Description
Circle trace (CTS)	Standing	Trace out a circle in the transverse plane with leg while in a standing position, rotating only at hip.
Front-side leg raise (FSS)	Standing	Alternating between leg raises to the front (sagittal) and side (coronal).
Circle trace (CTL)	Lying down	Tracing out a circle in the transverse plane, with minimum knee bending.
Straight-diagonal leg raise (SDR)	Lying down	Alternating between front leg extension (sagittal) and side leg extension (away from sagittal).

The subjects performed a series of exercises, as described in table 2, designed to model physiotherapy exercises. Each participant performed two sets of ten motions for each motion type.

However, due to the nature of the rehabilitation motions examined, the motions tested in table 2 are all sagittal plane motions. A second set of out-of-plane motions was collected with 1 male participant in order to verify the algorithm's capability to recover out-of-plane movement. The tested motions for this second set can be found in table 3.

For both datasets, the data were collected using the SHIMMER IMU (Burns *et al* 2010) sensor suite[5], which contains a Freescale MMA7361L 3D accelerometer, two InvenSense 2D IDG-500 gyroscopes mounted perpendicularly to each other to obtain 3D sensing, and a Roving Networks RN-42 Bluetooth radio. This sensor suite collects linear acceleration and angular velocity data, and transmits wirelessly via Bluetooth at 128 Hz. 3 SHIMMER devices were used, placed on (1) the hip, along the height of the anterior superior iliac spine (ASIS, a major bony landmark on the hip), at the mid-sagittal region of the subject, (2) on the thigh near the knee, and (3) on the calf, near the ankle. Figure 1 shows the placement of the SHIMMER sensors.

A calibration application based on Ferraris *et al* (1995) was provided by Shimmer Research, and was used to calibrate the accelerometer and gyroscope sensors. Ferraris' method was chosen as it is easy to apply, and does not require specialized equipment such as a turntable. The accelerometer sensitivity and bias are calculated by placing the sensor on a level surface

[5] Shimmer Research, www.shimmer-research.com

in the six different possible orientations and applying a linear regression to find the scaling parameters. The gyroscope bias and sensitivity are obtained by holding the gyroscope still and then rotating the sensor 360° around its three axes. Based on this measurement data, a bias vector and sensitivity matrix are computed.

Data were also simultaneously collected on a motion analysis motion capture system[6], with a sampling frequency of 60 Hz. Eight Eagle cameras were used, and the Motion Analysis Cortex software was used for data collection. Markers were placed on the SHIMMER sensors, the subject's shoulders, ASIS, right knee and ankle on both medial and lateral side, as well as the toe and heel. These markers were used to estimate the location of the SHIMMER sensors and joint centers for joint angle verification. The position of the knee and ankle were obtained by taking the average of their respective medial and lateral positions. Spline interpolation was applied to fill in occluded markers and the data were swept for switched markers. The data streams produced by SHIMMER and the Motion Analysis system were timestamped and time-aligned in post-processing.

The proposed EKF algorithm was applied to the SHIMMER data. The initial angles for the EKF were determined numerically by applying inverse kinematics to the Cortex data.

The initial noise profiles for the rehabilitation motion dataset were tuned to a single participant. That is, the five exercise motions of the reference patient were examined, and a single noise profile was derived across all five exercises. This noise profile was applied uniformly to all the exercises of the other 19 participants. For motions that were performed by other participants that may differ in speed, the auto-tuning mechanism described in section 2.3 is used to adapt the noise model. The kinematic constraint limits q_c were aggregated from several anthropometric joint limit tables (Norkin and White 2009, Bridger 2008). The kinematic link lengths were obtained from the motion capture marker information. The potential field coefficient η and the influence distance ρ_0 were set to 1 and 75% of the joint limits, respectively.

3.2. State estimation for rehabilitation motions

Prior to the accuracy analysis, two outlier motions were removed from the total set of 200 motion sets, due to a sensor error during data collection. To compare the results obtained from the EKF with the motion capture data, following estimation of the joint angles using the proposed algorithm, equations (6) and (7) were used to compute the Cartesian location of the IMU markers. The estimated locations of the knee and ankle sensors were compared to the motion analysis measured sensor locations, and the root mean square (RMS) computed. Table 4 presents the RMS for each Cartesian direction, as well as the average error for the upper (hip–knee) link, the lower (hip–ankle) link, and the total average error. The data were grouped together by motion type, with only the anthropometric joint limits as the kinematic constraints. The RMS data were also converted to joint angles, by applying the cosine rule to the link lengths and the RMS values. Table 4 also presents the joint angle errors for the upper (hip–knee) and the lower (knee–ankle) link.

Considering these results, it is evident that the largest errors exist in the z-axis (i.e. the motion out of the sagittal plane, cf figure 1), where there is little actual motion. Without strong motion in that direction, the estimation suffers from drift, causing a large reported RMS. In general, larger RMSes were reported in the lower leg than the upper leg. This is expected, as the end-effector distance errors from the upper leg are also implicitly included in the lower leg. Once again, the impact of drift can be observed strongly in the lower leg z-axis. With only

[6] Motion Analysis Corporation, www.motionanalysis.com

Table 4. EKF RMS results, by motion type, for the rehabilitation dataset, without any out-of-plane angle constraints. Cortex link length used. Results shown for each of the Cartesian dimensionality, as well as upper (U), lower (L) and total (T) errors. The degree error for the upper (U) and lower (L) joint is also shown.

	RMS (cm)									RMS (deg)	
	X1	Y1	Z1	X2	Y2	Z2	U	L	T	U	L
KF	3.98	1.58	5.53	4.39	3.45	8.49	3.70	5.44	4.57	6.01	4.12
SS	1.59	2.28	2.44	2.19	4.16	2.78	2.10	3.04	2.57	7.60	4.90
SQ	1.59	2.29	4.84	2.81	4.34	5.78	2.91	4.31	3.61	10.82	8.45
HF	5.01	3.18	5.00	5.88	4.35	8.52	4.40	6.25	5.32	6.28	4.86
SL	5.72	2.96	3.93	6.21	3.53	9.44	4.20	6.39	5.30	5.91	5.53
AVG	3.56	2.46	4.35	4.28	3.98	6.97	3.46	5.08	4.27	7.35	5.59

Table 5. EKF RMS results, by motion type, for the out-of-plane dataset. Results shown for each of the Cartesian dimensionality, as well as upper (U), lower (L) and total (T) errors. The degree error for the upper (U) and lower (L) joint is also shown.

	RMS (cm)									RMS (deg)	
	X1	Y1	Z1	X2	Y2	Z2	U	L	T	U	L
CTS	2.09	7.49	6.99	2.82	12.22	9.71	5.77	8.25	7.01	8.89	6.08
FSS	2.16	5.44	4.44	2.59	10.67	8.55	4.16	7.27	5.71	6.32	7.42
CTL	2.30	1.57	3.58	5.22	3.30	7.56	3.45	5.36	4.41	5.21	6.49
SDR	3.44	1.91	4.90	4.00	2.47	5.88	3.60	4.12	3.86	5.39	1.59
AVG	2.50	4.10	4.98	3.66	7.17	7.93	4.25	6.25	5.25	6.45	5.40

general anthropometric constraints, table 4 shows a total mean RMS of 4.27 cm, with 3.46 cm for the upper leg and 5.08 cm for the lower leg.

3.3. State estimation for out-of-plane motions

The RMS for the out-of-plane motions were calculated in the same manner as the rehabilitation motions. Table 5 presents the Cartesian and degree error by motion type. With a total Cartesian RMS of 5.25 cm and an upper and lower joint error of 6.45° and 5.40° respectively, the algorithm is shown to work with similar effectiveness with out-of-plane motions when compared to the in-plane rehabilitation motions.

Although only healthy participants were examined, the proposed algorithm is well suited to use on the rehabilitation population. The proposed algorithm does not assume any *a priori* knowledge of the movement that is being performed and functions identically for the sagittal-plane dataset and the out-of-plane dataset. No parameter modifications were made to apply the algorithm to each of the healthy participants, covering a range of movement speed and pattern. It is possible that, with the rehabilitation population, state noise covariance would need to be modified, but the mechanics of the algorithm would remain identical.

3.4. Comparison to existing approaches

Two alternative algorithms were also implemented to serve as comparison benchmarks: Boonstra *et al* (2006)'s implementation of the complementary filter and Luinge and Veltink (2005)'s implementation of the strapdown integrator. Similar to the proposed algorithm, the two comparison algorithms rely on accelerometers and gyroscopes to produce orientation

Table 6. EKF RMS results by motion type, for the rehabilitation dataset, comparing two other algorithms with the proposed. Errors reported in (cm). Results are given for the upper link (U), lower link (L) and total error (T).

	Boonstra			Luinge, no bias			Luinge, bias			Proposed		
	U	L	**T**	U	L	**T**	U	L	**T**	U	L	**T**
KF	3.13	6.83	**4.98**	2.78	4.53	**3.66**	2.51	3.82	**3.16**	2.51	3.48	**2.99**
SS	2.02	3.58	**2.80**	1.22	2.36	**1.79**	1.99	3.36	**2.67**	1.72	2.74	**2.23**
SQ	1.70	4.04	**2.87**	1.52	2.88	**2.20**	1.95	3.58	**2.76**	1.91	3.26	**2.69**
HF	6.18	8.24	**7.21**	4.12	4.86	**4.49**	4.06	4.79	**4.43**	3.90	4.50	**4.20**
SL	8.05	10.62	**9.33**	4.16	5.83	**5.00**	4.18	5.59	**4.88**	4.37	4.56	**4.47**
AVG	4.20	6.65	**5.42**	2.76	4.09	**3.42**	2.93	4.22	**3.58**	2.87	3.70	**3.31**

Table 7. EKF RMS results for the end-effector, by motion type, for the rehabilitation dataset, comparing two other algorithms with the proposed. Errors reported in (deg). Results are given for the local upper (U) and lower (L) joint errors.

	Boonstra		Luinge, no bias		Luinge, bias		Proposed	
	U	L	U	L	U	L	U	L
KF	5.02	8.48	4.59	4.23	4.11	3.15	4.13	1.67
SS	7.26	9.48	4.45	5.72	7.25	6.94	6.00	3.74
SQ	6.36	13.07	5.60	7.60	7.08	8.86	7.08	5.39
HF	8.83	5.01	5.88	2.08	5.75	1.96	5.55	1.53
SL	11.20	6.00	5.88	4.89	5.90	4.06	6.17	1.12
AVG	7.70	8.45	5.29	4.90	6.04	5.01	5.81	2.73

estimates. Both the accelerometer and the gyroscope are important, since the accelerometer returns accurate incline angles due to gravity, but is not reliable when the subject's motion acceleration is not negligible compared to gravity. The gyroscope can be integrated to obtain joint angles during faster movements, but suffers from integrational drift. Boonstra *et al* (2006)'s algorithm considers only sagittal motion, so comparisons to the proposed algorithm are made to the sagittal-only results, where out-of-plane angles were locked to the initial joint values. The Cartesian RMS results can be found in table 6, and table 7 for joint angle error.

Several minor modifications were made to Boonstra's algorithm for this comparison. Rather than using the parameters recommended by Boonstra, which may be optimized for their sensor suite, the filter parameters were optimized on the Shimmer devices in order to obtain the best possible performance. The sagittal incline angle was used to rotate the link lengths so that Cartesian RMS can be calculated for comparison against the proposed algorithm. Lastly, it was unclear how Boonstra combined the accelerometer-derived joint angle to the gyroscope-derived joint angle, so the average of the two was used.

From tables 6 and 7, it can be noted that Boonstra's algorithm does not perform as well as the proposed algorithm. The high-pass filter used in Boonstra does not perfectly eliminate the gyroscopic drift, which can be very significant. Without the accelerometer angle to average with, the reconstructed angles derived from the gyroscope would be very poor. This is the cause of numerous high-error entries for Boonstra in table 6, emphasizing that the high-pass filter is not sufficient. Boonstra also notes that the high-pass filter may be removing movement information from the sensors, which would also hurt the angle estimates. Lastly, Boonstra's algorithm does not provide a methodical way to combine the measurement sources, whereas the EKF calculates a weighing factor, the Kalman gain (equation (18)), to combine all the measured data appropriately.

Table 8. EKF RMS results, by motion type, for the out-of-plane dataset, using Luinge's algorithm without gyroscope bias. Results shown for each of the Cartesian dimensionality, as well as upper (U), lower (L) and total (T) errors. The degree error for the upper (U) and lower (L) joint is also shown.

	RMS (cm)									RMS (deg)	
	X1	Y1	Z1	X2	Y2	Z2	U	L	T	U	L
CTS	21.85	17.05	23.32	48.55	29.51	41.68	20.74	39.91	30.33	32.38	43.89
FSS	1.49	2.63	2.23	3.16	6.59	4.42	2.12	4.72	3.42	3.21	5.95
CTL	4.46	2.21	3.31	5.69	2.76	5.56	3.32	4.67	4.00	5.04	3.02
SDR	4.72	2.06	2.42	11.66	5.12	5.83	3.06	7.54	5.30	4.60	10.17
AVG	8.13	5.99	7.82	17.26	11.00	14.37	7.31	14.21	10.76	11.31	15.76

The second comparison algorithm considered was Luinge and Veltink (2005)'s implementation of the strapdown integration approach, where the movement and orientation of an object are estimated by rigidly attached IMUs, using a Kalman filter framework. The angles are determined by gyroscopic integration, which is then used to rotate and isolate the gravity vector from the inertial acceleration. The Kalman filter combines the sagittal incline angle derived from the acceleration signal with the integrated angles derived from the gyroscope signal. The sensor noise is explicitly modeled by the Kalman filter.

Luinge's algorithm also includes the gyroscope sensor dc bias as a Kalman state variable to address drift. Two implementations of Luinge's algorithm were constructed for the results shown in table 6, one with and one without gyroscope bias correction. The two implementations allow us to analyze the contribution of the kinematic model and the contribution of bias correction to the system performance separately. For the rehabilitation dataset, the gyroscope bias does not affect performance, since out-of-gravitation plane motion, which is most susceptible to drift, is restricted.

A full 3D DoF version of Luinge's algorithm was also implemented, to compare between Luinge's algorithm and the proposed algorithm in an unconstrained situation, using the out-of-plane motion dataset. Table 8 outlines the results from Luinge's algorithm in terms of Cartesian and joint angle error. Comparing the results for the proposed algorithm in table 5 and Luinge's algorithm in table 8, it can be seen that the performance in the sagittal plane is comparable, but the overall z-axis off-sagittal drift is much larger with Luinge's algorithm, resulting in a larger overall error reported for Luinge's algorithm. The inclusion of a kinematic model allows the proposed algorithm to constrain unfeasible motions that Luinge's algorithm does not, such as abduction motion in the knee. This allows the proposed algorithm to reduce drift.

Tables 9 and 10 show Luinge's algorithm with and without gyroscope bias, as well as the proposed algorithm in full 3D angle recovery without any sagittal constraints. Unlike the sagittal case, the inclusion of the gyroscope bias in Luinge's algorithm significantly improves performance in the case of unconstrained motion, particularly in the off-sagittal axis direction.

The performance of Luinge's algorithm is comparable to the proposed approach, showing the advantage of the principled integration of both sensor sources via the Kalman filter framework. However, with both comparison algorithms, only incline angles to the horizontal and heading angle to the vertical are estimated, while the proposed algorithm can estimate pose and report the results in the more clinically-relevant joint angle. Due to the lack of kinematic constraints, the comparison algorithms also allow drift in DoFs that are not physically feasible, which degrades the quality of the angle estimates.

Table 9. EKF RMS results by motion type, for the out-of-plane dataset, comparing Luinge's algorithm with the proposed. Errors reported in (cm). Results are given for the upper link (U), lower link (L) and total error (T).

	Luinge, no bias			Luinge, bias			Proposed		
	U	L	**T**	U	L	**T**	U	L	**T**
CTS	20.74	39.91	**30.33**	5.61	11.34	**8.47**	5.77	8.25	**7.01**
FSS	2.12	4.72	**3.42**	3.26	8.15	**5.71**	4.16	7.27	**5.71**
CTL	3.32	4.67	**4.00**	4.10	8.47	**6.29**	3.45	5.36	**4.41**
SDR	3.06	7.54	**5.30**	3.92	7.79	**5.86**	3.60	4.12	**3.86**
AVG	7.31	14.21	**10.76**	4.22	8.94	**6.58**	4.25	6.25	**5.25**

Table 10. EKF RMS results by motion type, for the out-of-plane dataset, comparing Luinge's algorithm with the proposed. Errors reported in (deg). Results are given for the local upper (U) and lower (L) joint errors.

	Luinge, no bias		Luinge, bias		Proposed	
	U	L	U	L	U	L
CTS	32.38	43.89	8.65	12.81	8.89	6.08
FSS	3.21	5.95	4.94	11.17	6.32	7.42
CTL	5.04	3.02	6.20	9.86	5.22	6.49
SDR	4.60	10.17	5.89	8.77	5.40	1.59
AVG	11.31	15.76	6.42	10.65	6.46	5.40

The error magnitudes obtained by the proposed algorithm are comparable to errors reported using goniometric systems. Chao (1980) reported a sagittal mean error of 1.4°, when comparing an electrogoniometer with x-ray data. Jagodzinski *et al* (2000) examined hip and knee goniometeric measurement accuracies against radiology images of the leg, and noted a mean degree error of 3.92° with a standard goniometer and 1.22° with a long-arm goniometer, with 3.3° of inter-rater variance between the two examiners. Edwards *et al* (2004) reports that mean error of goniometer measurement of knee angle ranged from 0° at 90° knee flexion, to 3° error at 120° flexion. The average error rose to an average of 5° error with unaided visual assessments. The corresponding joint error for the proposed algorithm reports a sagittal error of 2.73°, which makes it better then a joint assessment, and comparable to existing goniometric methods. This makes the proposed algorithm a viable alternative to the existing goniometer methods as the sensors are lightweight and do not require a brace such as those required by an electrogoniometer. It also provides joint angle estimates in both static and dynamic situations, providing exercise velocity and timing information that a goniometeric system would not be able to supply.

4. Conclusions and future work

This paper proposes an algorithm for estimating lower body pose based on inertial measurement units and the extended Kalman filter. With the assistance of kinematic constraints and noise covariance adjustments, the proposed system achieves an overall average RMS of 4.3 cm, and is capable of estimating joint angles accurately for arbitrary 3D motion of the lower leg.

For future work, motion data will be collected from joint replacement physiotherapy patients, in order to assess the system's accuracy against a test population whose motions may have different noise characteristics from a healthy population. More general motions that do not require a stationary base frame, such as gait, will be examined.

References

Bergmann J, Mayagoitia R and Smith I 2009 A portable system for collecting anatomical joint angles during stair ascent: a comparison with an optical tracking device *Dyn. Med.* **8** 1–7

Boonstra M C, van der Slikke R M A, Keijsers N L W, van Lummel R C, de Waal Malefijt M C and Verdonschot N 2006 The accuracy of measuring the kinematics of rising from a chair with accelerometers and gyroscopes *J. Biomech.* **39** 354–8

Bridger R S 2008 *Introduction to Ergonomics* (Boca Raton, FL: CRC Press) (available at http://www.crcpress.com/product/isbn/9780849373060)

Burns A, Greene B R, McGrath M J, O'Shea T J, Kuris B, Ayer S M, Stroiescu F and Cionca V 2010 Shimmer: a wireless sensor platform for noninvasive biomedical research *IEEE Sensors J.* **10** 1527–34

Chao E Y S 1980 Justification of triaxial goniometer for the measurement of joint rotation *J. Biomech.* **13** 989–1006

Dong W, Chen I M, Lim K Y and Goh Y K 2007 Measuring uniaxial joint angles with a minimal accelerometer configuration *Proc. Int. Convention on Rehabilitation Engineering and Assistive Technology* pp 88–91

Edwards J Z, Greene K A, Davis R S, Kovacik M W, Noe D A and Askew M J 2004 Measuring flexion in knee arthroplasty patients *J. Arthroplasty* **19** 369–72

Ferraris F, Grimaldi U and Parvis M 1995 Procedure for effortless in-field calibration of three-axial rate gyro and accelerometers *Sensors Mater.* **7** 311–30

Higgins W T 1975 A comparison of complementary and Kalman filtering *IEEE Trans. Aerosp. Electron. Syst.* **AES-11** 321–5

Howe J A, Inness E L, Venturini A, Williams J I and Verrier M C 2006 The Community Balance and Mobility Scale-a balance measure for individuals with traumatic brain injury *Clin. Rehabil.* **20** 885–95 (available at http://cre.sagepub.com/content/20/10/885.short)

Jagodzinski M, Kleemann V, Angele P, Schnhaar V, Iselborn K, Mall G and Nerlich M 2000 Experimental and clinical assessment of the accuracy of knee extension measurement techniques *Knee Surg. Sports Traumatol. Arthrosc.* **8** 329–36

Khatib O 1985 Real-time obstacle avoidance for manipulators and mobile robots *Proc. IEEE Conf. on Robotics and Automation* pp 500–05

King A D 1998 Inertial navigation—forty years of evolution *Gen. Electr. Co. Rev.* **3** 140–9 (available at http://www.imar-navigation.de/downloads/papers/inertial_navigation_introduction.pdf)

Luinge H and Veltink P 2005 Measuring orientation of human body segments using miniature gyroscopes and accelerometers *Med. Biol. Eng. Comput.* **43** 273–82

Norkin C C and White D J 2009 *Measurement of Joint Motion: A Guide to Goniometry* 4th edn (Philadelphia, PA: F. A. Davis Company) (available at http://www.fadavis.com/product/physical-therapy-measurement-joint-motion-goniometry-norkin-white-4)

Roetenberg D, Baten C T M and Veltink P H 2007 Estimating body segment orientation by applying inertial and magnetic sensing near ferromagnetic materials *IEEE Trans. Neural Syst. Rehabil. Eng.* **15** 469–72

Roetenberg D, Luinge H and Slycke P J 2009 Xsens mvn: full 6dof human motion tracking using miniature inertial sensors *Technical report* (Xsens Technologies) (available at http://www.xsens.com/images/stories/PDF/MVN_white_paper.pdf)

Spong M W, Hutchinson S and Vidyasagar M 2006 *Robot Modeling and Control* (New York: Wiley) (available at http://ca.wiley.com/WileyCDA/WileyTitle/productCd-EHEP000518.html)

Uicker J J Jr, Denavit J and Hartenberg R S 1964 An iterative method for the displacement analysis of spatial mechanics *J. App. Mech.* **31** 309–14

Wan E A and Nelson A T 2001 Dual EKF methods *Kalman Filtering and Neural Networks* (New York: Wiley) pp 123–73 (available at http://ca.wiley.com/WileyCDA/WileyTitle/productCd-0471369985.html)

Welch G and Bishop G 2006 *An Introduction to Kalman Filters Technical Report* (Chapel Hill: University of North Carolina) (available at http://www.cs.unc.edu/∼welch/media/pdf/kalman_intro.pdf)

Williamson R and Andrews B J 2001 Detecting absolute human knee angle and angular velocity using accelerometers and rate gyroscopes *Med Biol. Eng. Comput.* **39** 294–302

Zhou H, Stone T, Hu H and Harris N 2008 Use of multiple wearable inertial sensors in upper limb motion tracking *Med. Eng. Phys.* **30** 123–33

Zhu R and Zhou Z 2004 Realtime articulated human motion tracking using tri-axis inertial/magnetic sensors package *IEEE Trans. Neural Syst. Rehabil. Eng.* **12** 295–302